Bioactive Materials 6 (2021) 447–459

Contents lists available at ScienceDirect

Bioactive Materials

journal homepage: http://www.keaipublishing.com/biomat

Inhibition of bacterial adhesion and biofilm formation by a textured fluorinated alkoxyphosphazene surface

Meixian Tang[a], Chen Chen[b], Jieru Zhu[b], Harry R. Allcock[b], Christopher A. Siedlecki[a,c], Li-Chong Xu[c,*]

[a] Department of Biomedical Engineering, The Pennsylvania State University, University Park, PA, 16802, United States
[b] Department of Chemistry, The Pennsylvania State University, University Park, PA, 16802, United States
[c] Department of Surgery, The Pennsylvania State University, College of Medicine, Hershey, PA, 17033, United States

ARTICLE INFO

Keywords:
Fluorinated polyphosphazene
Textured surface
Crosslinking
Anti-bacterial adhesion
Anti-biofilms
Microbial infection

ABSTRACT

The utilization of biomaterials in implanted blood-contacting medical devices often induces a persistent problem of microbial infection, which results from bacterial adhesion and biofilm formation on the surface of biomaterials. In this research, we developed new fluorinated alkoxyphosphazene materials, specifically poly[bis(octafluoropentoxy) phosphazene] (OFP) and crosslinkable OFP (X–OFP), with improved mechanical properties, and further modified the surface topography with ordered pillars to improve the antibacterial properties. Three X–OFP materials, X–$OFP_{3.3}$, X–$OFP_{8.1}$, X–$OFP_{13.6}$, with different crosslinking densities were synthesized, and textured films with patterns of 500/500/600 nm (diameter/spacing/height) were fabricated via a two stage soft lithography molding process. Experiments with 3 bacterial strains: *Staphylococcal epidermidis, Staphylococcal aureus*, and *Pseudomonas aeruginosa* showed that bacterial adhesion coefficients were significantly lower on OFP and X–OFP smooth surfaces than on the polyurethane biomaterial, and surface texturing further reduced bacterial adhesion due to the reduction in accessible surface contact area. Furthermore the anti-bacterial adhesion effect shows a positive relationship with the crosslinking degree. Biofilm formation on the substrates was examined using a CDC biofilm reactor for 7 days and no biofilm formation was observed on textured X–OFP biomaterials. The results suggested that the combination of fluorocarbon chemistry and submicron topography modification in textured X–OFP materials may provide a practical approach to improve the biocompatibility of current biomaterials with significant reduction in risk of pathogenic infection.

1. Introduction

Medical devices such as prosthetics, catheters, valves, and stents, are an indispensable component in the practice of modern medicine. However, implant infection is one of the most frequent and severe complications associated with the use of biomaterials in the medical devices [1]. According to recent statistics, device-associated infections account for approximately 25.6% of all healthcare associated infections, lead to increased patient morbidity and mortality, and impose a huge financial burden on healthcare services in the USA [2]. The emergence of microbial infections on medical devices is associated with bacterial adhesion and then formation of a protective biofilm. The common microorganisms associated with implant infections include Gram-positive bacteria such *Staphylococcus aureus*, *Staphylococcus epidermidis* and *Enterococcus faecalis*; and Gram-negative bacteria, e.g., *Escherichia coli, Klebsiella pneumoniae, Proteus mirabilis* and *Pseudomonas aeruginosa*. The growth of these microorganisms within biofilms often poses a challenge in treating the infections [3].

Current clinical treatments of microbial infections rely on use of large quantities of antibiotics, but the increasing tolerance to antibiotics and biofilm formation often make device-centered infections difficult to treat. In fact, the rapid emergence and dissemination of resistance among bacterial pathogens have led to a crisis in healthcare [4–6]. An alternative to combatting microbial infection on devices is to impart surfaces with antibacterial properties to reduce bacterial attachment and proliferation via surface coating or surface modification [7,8]. These surfaces generally use two different mechanisms, either containing biocidal compounds (e.g. metal nanoparticles) to inactivate any cells coming into contact with the surface [9], or having hydrophilic, highly hydrated, non-charged polymers such as poly (ethylene glycol)

Peer review under responsibility of KeAi Communications Co., Ltd.
* Corresponding author. The Pennsylvania State University, College of Medicine, Mail code H151, 500 University Drive, Hershey, PA, 17033, United States.
E-mail address: lxx5@psu.edu (L.-C. Xu).

https://doi.org/10.1016/j.bioactmat.2020.08.027
Received 8 July 2020; Received in revised form 26 August 2020; Accepted 29 August 2020

(PEG) and its derivatives [10,11] or zwitterion-containing polymers [12] to inhibit the initial bacterial attachment. Another approach to generate antibacterial surfaces is physical surface modification with micro- and nanoscale surface topographical features, and the related nanotechnology to develop these materials has become an area of intense research focus [13,14]. These surfaces, either inspired from natural antifouling surfaces or engineered, have been recognized to play an important role in controlling bacterial attachment with the reduction of surface contact area for interaction with cells and/or changes in surface wettability with superhydrophobic or superhydrophilic properties. Another study showed that a natural nanopatterned structure on cicada wings has a bactericidal effect by inducing mechanical rupture [15], and biomimetic surfaces which contain high aspect ratio nanoprotrusions based on the structure of the wings of the dragonfly exhibited highly bactericidal effects against both Gram-negative and Gram-positive bacteria, along with endospores, independent of chemical composition [16]. Over the past few years, we have developed submicron textured polyurethane (PU) surfaces consisting of ordered arrays of pillars and showed that they exhibit resistance to bacterial adhesion/biofilm formation when fabricated in polymer surfaces [17,18]. Furthermore, these surfaces also showed resistance to platelet adhesion and plasma coagulation [19]. These results demonstrated the potential of surface topographic modification for use in clinical applications to combat health-care infections and thrombosis caused by implanted devices. However, to achieve an appropriate combination of properties the choice of a suitable polymeric substrate is crucial.

Among all the synthetic polymers that are known, polyphosphazenes offer one of the broadest means for controlling bulk and surface properties through synthetic chemistry. Polyphosphazenes are high polymers with a backbone of alternating phosphorous and nitrogen atoms and with various organic or inorganic side groups attached to the phosphorus atoms. Different side groups generate different inherent properties in polyphosphazene materials and provide wide applications potential in a variety of fields [20]. Polyphosphazenes can be designed to be biocompatible, biostable or biodegradable in aqueous media by varying the side groups that are attached to the backbone, and can be widely utilized as biomaterials in different biomedical environments. For example, bioerodible polyphosphazenes have been developed and utilized for drug delivery and as matrices for tissue generations [21]. Biodegradable polyphosphazenes containing fluoroquinolone antibiotic substituents [22] or S-nitrosothiol functional groups that release nitric oxide [23,24] have been proposed for antimicrobial infections. An important biostable polyphosphazene thermoplastic, poly[bis(trifluoroethoxy)phosphazene] (TFE), has been shown to exhibit biocompatible, anti-inflammatory, and antithrombogenic properties [25,26], and been used for coating of stents, resulting in reduced thrombus formation *in-vivo* [27–29]. However, the inherently poor elastomeric properties of TFE limits its applications in medical devices such as catheters. To eliminate this weakness and enhance the biocompatibility we synthesized several new fluorinated alkoxyphosphazenes – specifically poly[bis(octafluoropentoxy) phosphazene] (OFP) and a series of crosslinkable OFP (X–OFP) based on the TFE platform, where octafluoropentoxy side units are present at both functional sites along the backbone rather than having two trifluoroethoxy groups on each phosphorus as in TFE. We also introduced a limited number of allylphenoxy group side units to make the OFP crosslinkable [30]. Our results show that the fluorocarbon chemistry of OFP and X-OFPs is resistant to bacterial adhesion and biofilm formation, as well as reducing plasma coagulation and platelet adhesion/activation, which indicates an improvement in biocompatibility. In our most recent study we find that the crosslinking improved the mechanical properties of materials and made it feasible for shaped medical devices such as catheters, as well as permitting further surface topography modification. Furthermore, we found that the increase in material stiffness decreased the bacterial adhesion responses [31]. Extending from the previous findings, these results suggest that the combination of surface fluorocarbon chemistry, stiffness, and submicron topography modification in polyphosphazenes may significantly improve the resistance to microbial infection and largely increase the biocompatibility.

Thus, in our previous study we developed surface topography modification techniques with OFP and X–OFP surfaces and demonstrated their resistance to adhesion and biofilm formation of *S. epidermidis*, and blood coagulation [30]. In this study we synthesized additional X-OFPs with different crosslinking levels and utilized a surface topography modification with submicron pillars to investigate the bacterial adhesion and biofilm formation of three strains, *S. epidermidis, S. aureus, and P. aeruginosa*, on these surfaces. Three X-OFPs with different crosslinking degrees, X–$OFP_{3.3}$, X–$OFP_{8.1,}$ and X–$OFP_{13.6}$, were synthesized and modified with surface texturing, and the results show a negative correlation between bacterial attachment and increasing degrees of crosslinking, and no biofilm formations on textured X–OFP surfaces after 7 days.

2. Materials and methods

2.1. Synthesis of poly[bis(octafluoropentoxy) phosphazene] (OFP) and crosslinkable poly[bis(octafluoropentoxy) phosphazene] (X–OFP)

The syntheses of OFP and X-OFPs were carried out using standard Schlenk line techniques under a dry argon atmosphere. Glassware was dried for 24 h in an oven at 111 °C before use. The solvents used in reactions include tetrahydrofuran (THF, EMD) and diethyl ether, which were dried using a solvent purification system in which the solvents pass through columns of molecular sieves under a dry argon atmosphere. The reactants, 2-Allylphenol and 2,2,3,3,4,4,5,5-Octafluoro-1-pentanol (Aldrich), were distilled over calcium hydride. Poly (dichlorophosphazene) was prepared via the thermal ring-opening polymerization of recrystallized and sublimed hexachlorocyclotriphosphazene (Fushimi Pharmaceutical Co., Japan) in evacuated Pyrex tubes at 250 °C. Sodium hydride (60% dispersion in mineral oil, Aldrich) was used as received.

OFP and X-OFPs were synthesized following the procedures which have been described elsewhere [30,32] and the general synthesis routes to OFP and X-OFPs can be found in our previous publication [31]. Briefly, synthesis was carried out by dropwise addition of NaOAP to a solution of poly (dichlorophosphazene) in THF. The mixture was stirred for 16 h at room temperature, followed by dropwise addition of NaOOFP and stirred for additional 16 h at room temperature. The products were concentrated under reduced pressure, precipitated from THF into water three times and from THF into hexane three times, and finally dried under high vacuum (Scheme 1). In this study we synthesized three X-OFPs with different

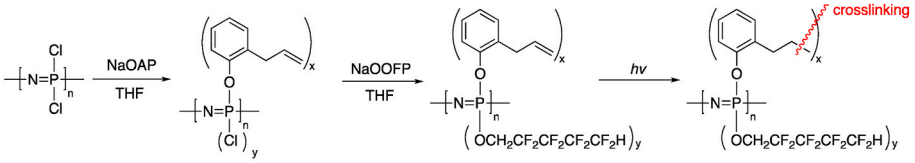

Scheme 1. Synthesis route of X–OFP polymers and crosslinking reactions under UV. (x = 0.066, y = 1.934 for X–$OFP_{3.3}$, x = 0.162, y = 1.838 for X–$OFP_{8.1}$, and x = 0.272, y = 1.728 for X–$OFP_{13.6}$).

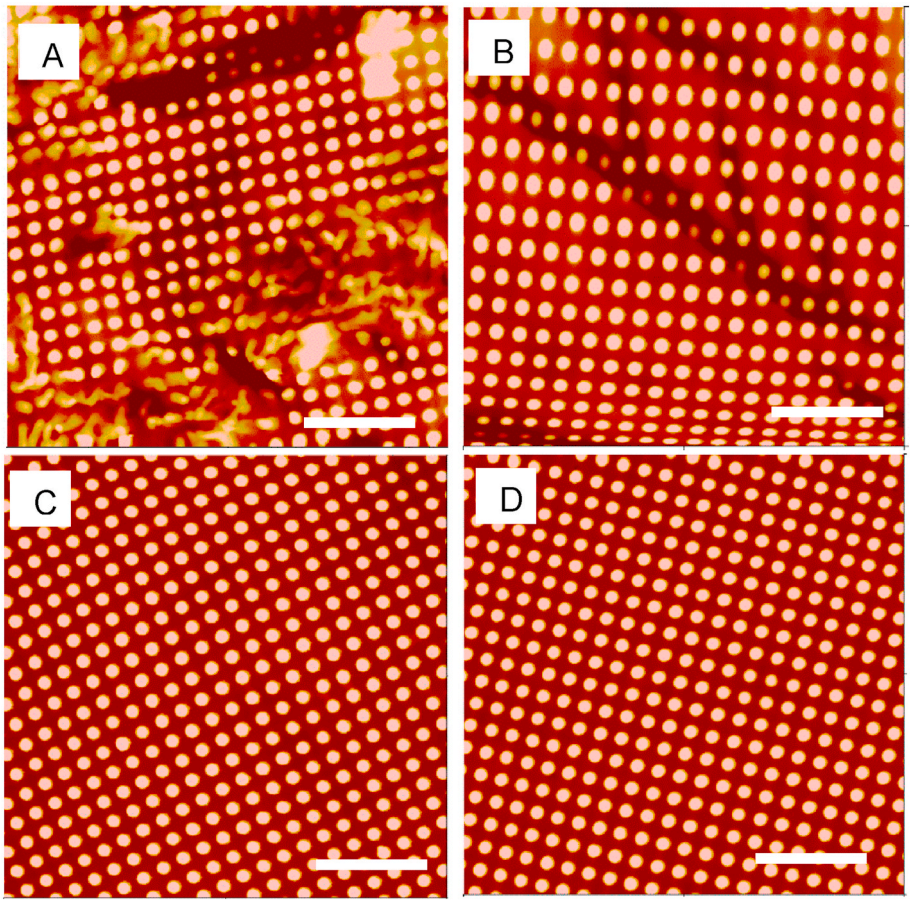

Fig. 1. AFM topography images of textured patterns of X–OFP$_{3.3}$ with solvent (A) DMAC, (B) DMF, (C) THF, and (D) MEK. All patterns are 500/500/600 nm pillars, scale bar = 5 μm, image scan area 20 × 20 μm^2. Defects were found on DMAC- or DMF- solvent textured films, no defects were observed on THF and MEK- films.

crosslinking densities: Poly [(2-allylphenoxy)$_{0.066}$ (2,2,3,3,4,4,5,5-Octafluoro-1-pentanoxy)$_{1.934}$phosphazene], Poly [(2-allylphenoxy)$_{0.162}$ (2,2,3,3,4,4,5,5-Octafluoro-1-pentanoxy)$_{1.838}$phosphazene], and Poly [(2-allylphenoxy)$_{0.272}$ (2,2,3,3,4,4,5,5-Octafluoro-1-pentanoxy)$_{1.728}$phosphazene], containing 3.3, 8.1, and 13.6% crosslinkable functional groups, respectively. Thereafter we named them as X–OFP$_{3.3}$, X–OFP$_{8.1}$, and X–OFP$_{13.6}$, respectively. The structures of OFP and X-OFPs were confirmed by ^{1}H and ^{31}P NMR spectroscopy using a Bruker AV-360 instrument operated at 360 and 145 MHz, respectively. These results have been published elsewhere [31].

2.2. Preparation of textured polyphosphazene films with submicron pillars

The textured polyphosphazene film surfaces were fabricated with a modified soft lithography two-stage replication molding technique. The detailed procedures can be found in our previous publications [17,19]. Briefly, a master pattern with ordered arrays of pillars with dimensions of 500/500/600 nm (diameter/space distance between pillars/height) was first fabricated on a silicon wafer obtained from RTI International (Research Triangle Park, NC). Then polydimethylsiloxane (PDMS) was cast against the master pattern and cured in vacuum at 65 °C overnight to generate the negative silicone mold. OFP (~10% (w/v)) and X–OFP (~4% (w/v)) solutions were prepared in dimethylacetamide (DMAC), dimethylformamide (DMF), methyl ethyl ketone (MEK), and tetrahydrofuran (THF), respectively, for choosing the best solvent for the casting procedure. Polymers were dissolved in solvents with stirring for 12 h, and azobisisobutyronitrile (AIBN, Sigma-Aldrich) (5% (w/w)) was added to X–OFP solutions as the initiator for crosslinking reaction. The PDMS molds were treated in glow discharge air plasma cleaner (PDC-001, 200 W, Harrick Plasma, Ithaca, NY) for 30 s to increase the polyphosphazene solution's affinity to silicone molds. The polymer solution was cast on the mold and cured under vacuum overnight at room temperature. At least two additional layers were added and each layer was dried and cured at room temperature under vacuum, with additional subsequent layers added as necessary to reach the desired thickness. The thickness of films in this study is in the range of 100–300 μm. To crosslink X-OFPs, the X–OFP films on silicone molds were placed in a UV reactor with wavelength 254 nm under continuous N_2 flow for at least 2 h. Finally, all the molds with films were soaked in Millipore water and the films were separated, dried, and stored in petri dishes prior to use.

2.3. Measurement of surface wettability

A Krüss contact angle goniometer was used to measure the advancing water contact angle (θ) of polyphosphazene film surfaces to determine the surface wettability. All measurements were made using Millipore water as a probe liquid with an ~8 μL water droplet used for the measurement. Contact angles were measured by a minimum of eight independent measurements and are presented as mean ± standard.

2.4. Characterization of surface topography

The polymer films were cut into pieces with diameter of 10 mm and used for surface topography characterization by a multimode atomic force microscope (AFM) with a Nanoscope IIIa control system (Veeco, Santa Barbara, CA). AFM was operated in tapping mode (intermittent contact) in air using Si probes (NSG30_SS, TipsNano) with an aspect ratio > 3.5, tip curvature radius < 5 nm and drive

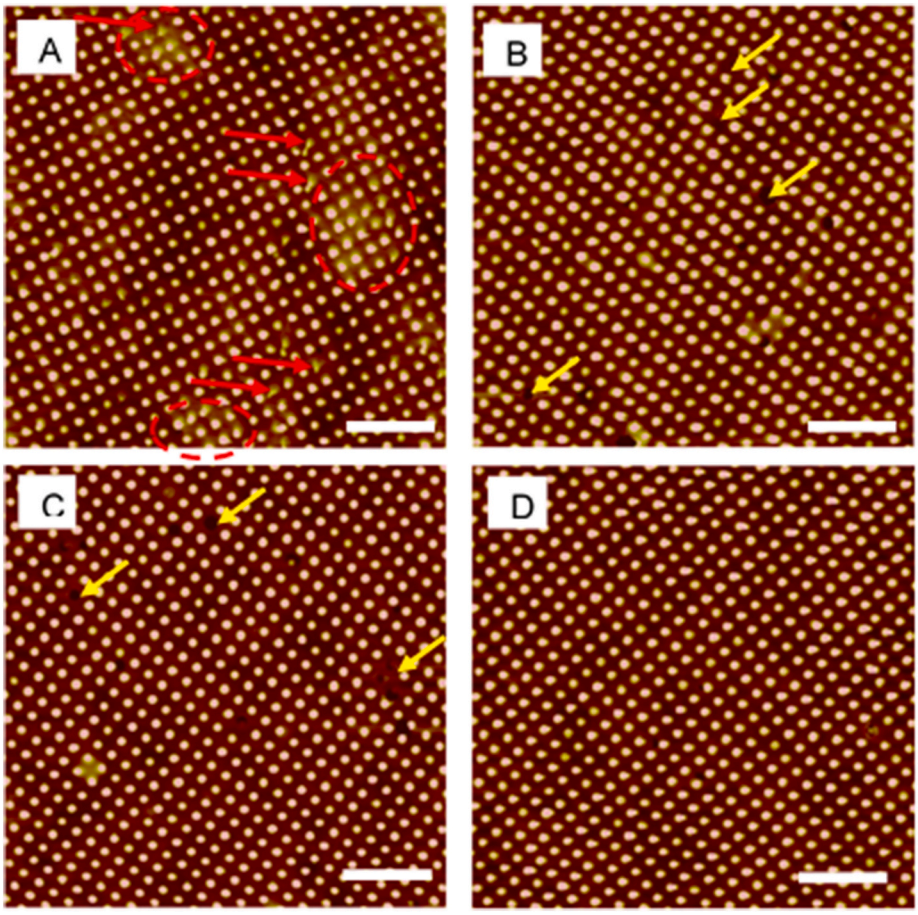

Fig. 2. AFM Topography images of textured materials with 500/500/600 nm patterns. (A) OFP, (B) X–$OFP_{3.3}$, (C) X–$OFP_{8.1}$ and (D) X–$OFP_{13.6}$. The red circles indicate areas with an underlying surface topography. The red arrows indicate collapsed pillars and yellow arrows indicate missing pillars. (Scale bar = 5 μm, image scan area 25 × 25 μm^2). (For interpretation of the references to color in this figure legend, the reader is referred to the Web version of this article.)

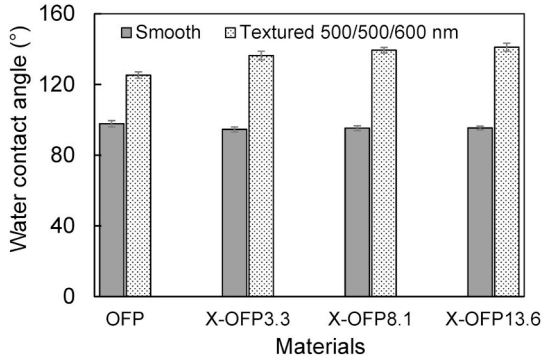

Fig. 3. Water contact angles of various polyphosphazene smooth and textured surfaces.

frequency ~ 180 kHz. Each sample was measured at no less than 3 different random locations.

2.5. Assessment of bacterial adhesion on polyphosphazene surfaces

Gram-positive *S. epidermidis* RP62A (ATCC 35984) and *S. aureus* Newman (ATCC 25904), and Gram-negative *P. aeruginosa* (ATCC 27853) were selected for adhesion responses to the material surfaces. Each strain was cultured at 37 °C in media with shaking at 250 rpm for 24 h in a shaking incubator (Corning, New York), and harvested by centrifugation at 1500*g* for 10 min. The bacterial cell pellets were re-suspended in phosphate-buffered saline (PBS, 0.01 M, pH 7.4, Sigma) and filtered through a 30-gauge needle to reduce bacterial aggregates. The concentration of bacteria was determined by turbidity measurements at 600 nm (OD_{600}) using a spectrophotometer. The polymer films were cut into round pieces with a diameter of 10 mm and attached in a Petri dish (100 mm × 25 mm). Each dish contained all different sample types which were distributed uniformly, and three replicate samples for each material were tested in separate petri dishes in every experiment. Samples were pre-soaked in PBS at 37 °C for 2 h to fully equilibrate the outermost surface of the polymer films. Bacterial solution (40 mL) with a concentration of 1×10^8 CFU/mL in PBS then replaced the PBS in the Petri dish and incubated for 1 h at 37 °C with a shake rate of 90 rpm in a Corning® LSE™ 71 L shaker. After 1 h, the bacteria solution was gently replaced with 40 mL PBS for 5 times, followed by fixing in 2.5% glutaraldehyde for 2 h. After being rinsed with PBS, the samples were stained with Hoechst (Invitrogen) and analyzed under a fluorescence optical microscope (Nikon, Eclipse 80i). For comparison, Biospan polyurethane (PU) MS/0.4 smooth films were prepared with the same method and used as a control in all experiments since it has been widely used in biomedical devices.

2.6. Assessment of biofilm formation on polyphosphazene surfaces

The three above-mentioned bacteria strains were used to investigate the biofilm formation on polyphosphazene film surfaces. A CDC biofilm reactor (Biosurface Technologies, Bozeman, MT) was used for evaluation of resistance to biofilm formation based on standard ASTM E2562 – 17. All culturing equipment, the CDC bioreactor and coupon holders were autoclaved before use. Polymer samples were cut into round pieces with a diameter of 12 mm and were attached to coupon holders. The reactor containing 10% culturing medium was inoculated with ~1×10^8 CFU/mL bacteria at 37 °C with stirring at 150 rpm. Every 24 h, 25% of the culturing medium was replaced with fresh medium to supplement nutrients. After 7 days, samples were lightly rinsed in sterile PBS buffer to remove non-adherent material and then stained

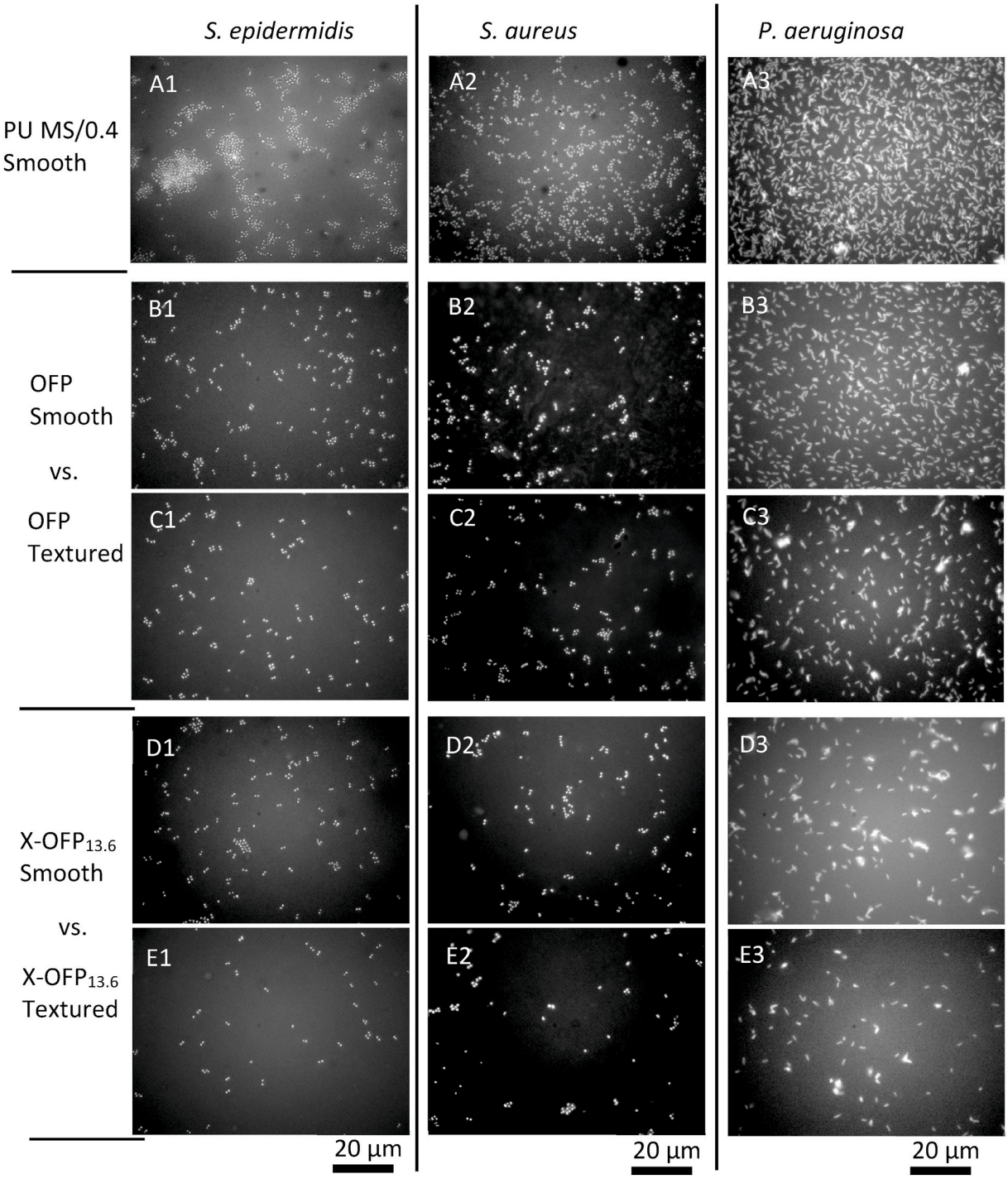

Fig. 4. Representative optical images of bacterial adhesion on PU MS/0.4 smooth, OFP smooth and textured, X–$OFP_{13.6}$ smooth and textured surfaces in PBS for 1 h.

with 100 μg/mL wheat germ agglutinin-FITC (Sigma) for 1 min, and fixed in 1% paraformaldehyde for 30 min. The samples were then examined by fluorescence optical microscopy.

2.7. Statistical analysis

Statistical analysis was performed using Minitab software (version 18). All data are reported as the mean ± standard deviation (n = 3 or more). Means of experimental data were compared by a 2-sample *t*-test and differences were considered statistically significant for $p < 0.05$. Significance is denoted with one symbol denoting $p < 0.05$, two symbols denoting $p < 0.01$, and three symbols denoting $p < 0.001$.

3. Results

3.1. Fabrication and characterization of textured OFP and X–OFP films

Uncrosslinked OFP and X-OFPs can be dissolved in many solvents such as dimethylacetamide (DMAC), dimethylformamide (DMF), methyl ethyl ketone (MEK), and tetrahydrofuran (THF) to fabricate the textured films by solvent evaporation. Fig. 1 illustrates the AFM surface topography images of textured X–$OFP_{3.3}$ films using these solvents by soft lithography two-stage replication molding technique with the pattern bearing ordered pillars of 500/500/600 nm. Many defects such as collapse and deformation of pillars were observed on the films using

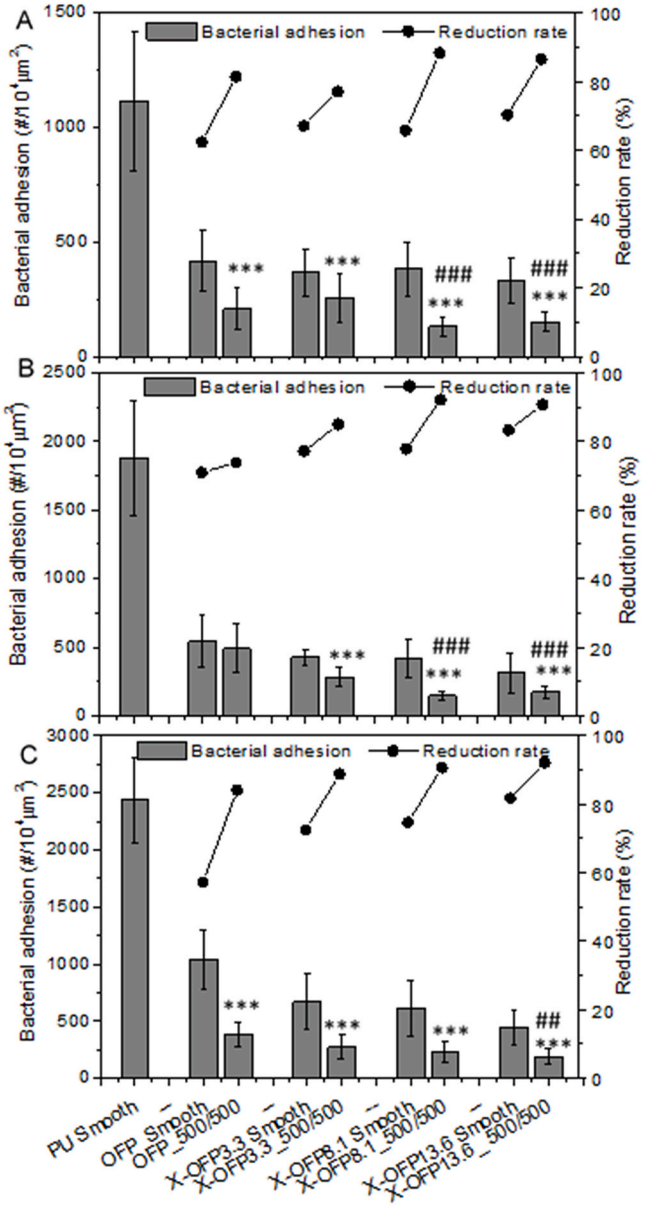

Fig. 5. Bacterial adhesion on polyphosphazene surfaces in PBS for 1 h, compared to adhesion on PU MS/0.4 surface, (A) *S. epidermidis*, (B) *S. aureus*, and (C) *P. aeruginosa*. Statistical symbol ***: $p < 0.001$, comparing smooth vs. textured for each material. ##: $p < 0.01$; ###: $p < 0.001$, comparing to textured X–$OFP_{3.3}$.

DMAC and DMF as solvents (Fig. 1A and B), while the THF- and MEK-solvent X–OFP films did not show these defects. Comparing the THF- and MEK- films, the THF-film appeared nontransparent and the structure was non-uniform, while the MEK-derived film was clear and uniform. Overall, these results suggest that MEK is the best among these solvents for dissolving OFP and X-OFPs for fabrication of textured polyphosphazene films.

Textured films were fabricated with OFP and crosslinked X–$OFP_{3.3}$, X–$OFP_{8.1}$ and X–$OFP_{13.6}$ materials using MEK as solvent (Fig. 2). The AFM topography images show the normal textured topographies obtained on materials, with occasional defects observed. On OFP surface, high level bumps indicated with light color in background were observed, suggesting that OFP material may produce a non-uniform substrate for the pillar texture (red circles in Fig. 2A). Furthermore, some pillars were found thin and collapsed as indicated with red arrows in Fig. 2A. By counting such collapsed pillars, approximately 3.9% defects were observed on OFP textured surface. Comparing with OFP, the X–OFP materials appear as uniform substrates for the textured pillars, particularly for X–$OFP_{8.1}$ and X–$OFP_{13.6}$, suggesting that the crosslinking reaction in X-OFPs produced good replicates of textured pattern from the master Si wafer. However, a few missed pillars were still observed on textured X–OFP surfaces, with rates of 1.33%, 1.05% and 0.27% pillars missing on X–$OFP_{3.3}$, X–$OFP_{8.1}$ and X–$OFP_{13.6}$ surfaces, respectively (yellow arrows in Fig. 2B–C). These results suggest that the increase in crosslinking density increased the mechanical strength of pillars and decreased the defects (missed pillars in this case) on textured surface structure.

The crosslinking treatment may affect the size of pillars. An X–$OFP_{13.6}$ film was chosen and characterized by AFM before and after crosslinking. The images were treated with ImageJ software and the diameter of pillar was analyzed from its projection area. Results show that the mean diameters of pillars were 536.8 ± 17.6 nm before crosslinking, and 508.7 ± 18.4 nm after crosslinking. The slight decrease of pillar diameters demonstrated that crosslinking of polymers may shrink the volume of material. However, this difference is so small compared to the normal size of pillars that it can be neglected in the subsequent influences on bacterial adhesion.

3.2. Surface wettability

OFP and X–OFP materials are normally hydrophobic due to the fluorocarbon chemistry. The mean water contact angle of OFP was 97.8 ± 1.75°. The incorporation of allylphenoxy groups and crosslinking reactions have no significant effect on wettability. The average water contact angles varied in the range of 93–97°. The surface texturing significantly raised the water contact angle due to the Cassie – Baxter effect, resulting from the air entrapped between pillars [33]. The water contact angles for corresponding textured X–OFP surfaces increased to 136.4 ± 2.5°, 139.4 ± 1.6°, and 141.4 ± 2.3°, respectively (Fig. 3).

3.3. Bacterial adhesion on OFP and X–OFP surfaces

Bacterial adhesion responses to textured polyphosphazene biomaterials were assessed in PBS solution containing bacteria for 1 h at low shaking speed. Since polyurethane biomaterials are widely used in current medical devices, we selected a representative PU MS/0.4 as the control for comparison in this study. Three representative hospital infection strains were assessed. Fig. 4 illustrates demonstrative images of bacterial adhesion on PU MS/0.4, OFP, and X–$OFP_{13.6}$ smooth and textured surfaces. Significant bacterial adhesion was observed on all PU MS/0.4 smooth surfaces. *S. epidermidis* adhered in clusters on the PU surface while *P. aeruginosa* adhesion was more uniform (Fig. 4A1-A3). Comparing to PU MS/0.4 counterparts, both smooth and textured OFP and X–OFP surfaces showed significantly reduced bacterial adhesion. Furthermore, lower adhesion was observed on textured surfaces compared to a smooth surface for each material. All adhesion data and reduction rates (vs. PU MS/0.4 smooth) are compiled and illustrated in Fig. 5. For *S. epidermidis*, bacterial adhesion reduction rates on OFP and X–OFP smooth surfaces varied over the range of 62–70% and the crosslinking degree has no significant effect on adhesion. The surface texturing further significantly reduced bacterial adhesion ($p < 0.001$) and the highest reduction rates were observed on textured X–$OFP_{8.1}$ and X–$OFP_{13.6}$ surfaces (88.3% and 87.5%, respectively) (Fig. 5A). It is interesting to see that both textured X–$OFP_{8.1}$ and X–$OFP_{13.6}$ surfaces exhibited significantly lower adhesion than textured X–$OFP_{3.3}$, suggesting that crosslinking density may be an important parameter in inhibition of bacterial adhesion by surface texturing. For *S. aureus* adhesion, smooth OFP and X–OFP materials reduced bacterial adhesion in the range from 71% to 83% and the textured surface reduced bacterial adhesion from 73% to 91% (Fig. 5B). Similar to *S. epidermidis*, high crosslinking density of textured surfaces leads to significantly lower

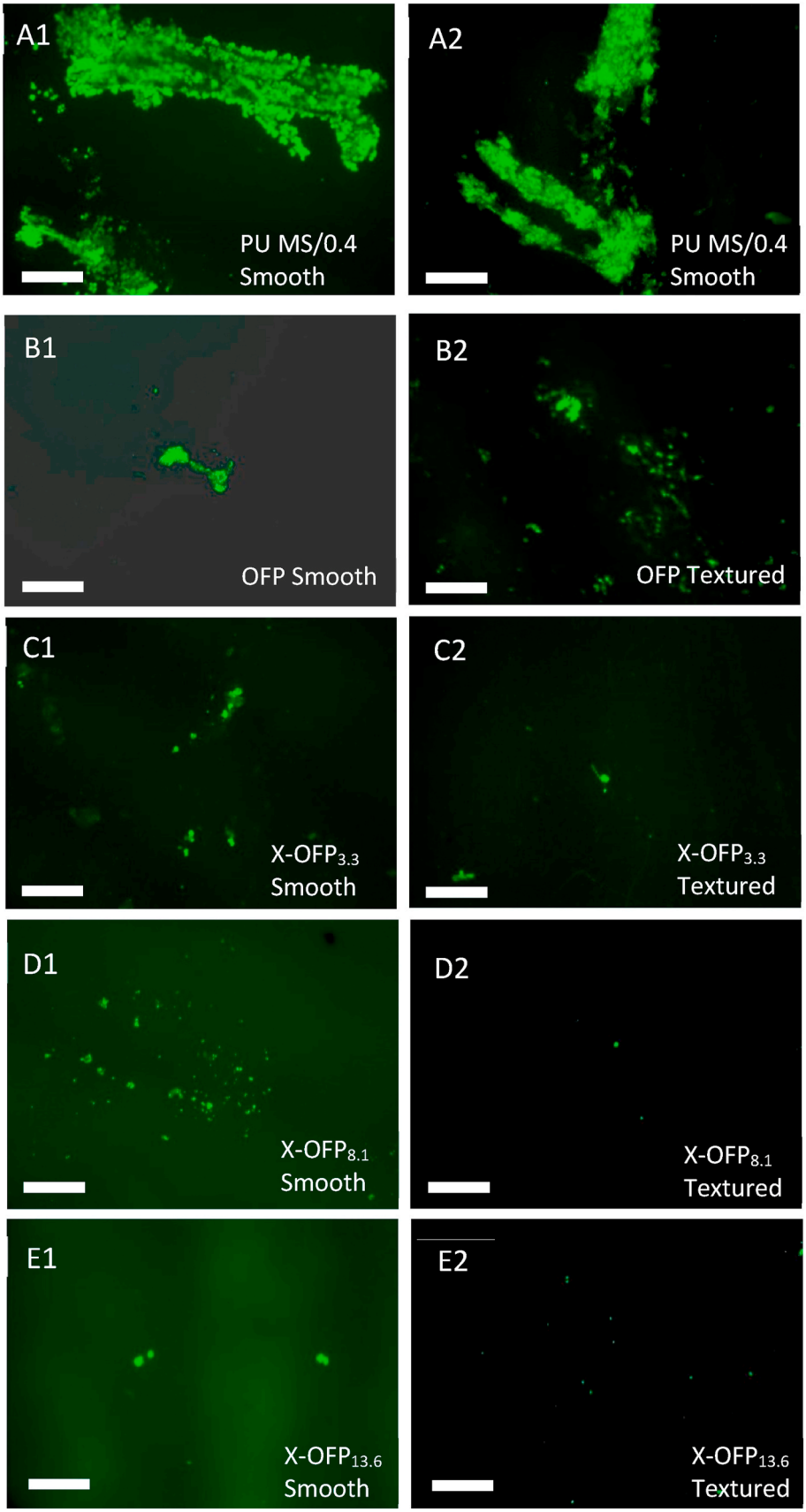

Fig. 6. Representative fluorescence images of material surfaces incubated in *S. epidermidis* culture in CDC biofilm reactor for 7 days. (A1, A2) PU MS/0.4 smooth, (B1, B2) OFP, (C1, C2) X–$OFP_{3.3}$, (D1, D2) X–$OFP_{8.1}$, (E1, E2) X–$OFP_{13.6}$. The textured surfaces were patterned with 500/500/600 nm pillars. (200 × , Scale bar = 50 μm).

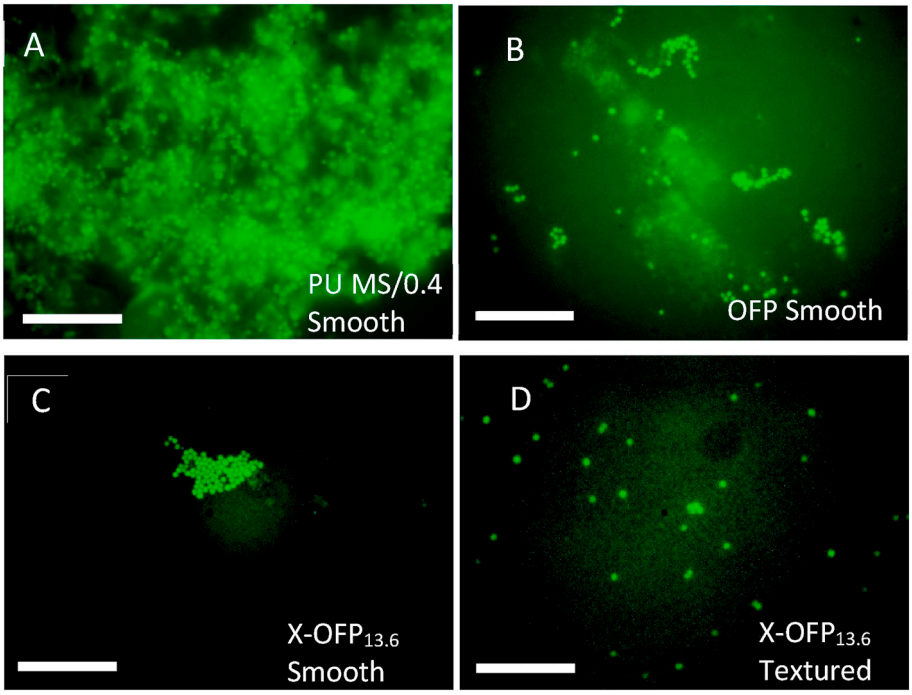

Fig. 7. Magnified fluorescence microscopy images of biofilms formed on (A) PU MS/0.4 smooth, (B) OFP smooth, (C) X–$OFP_{13.6}$ smooth and (D) X–$OFP_{13.6}$ textured surfaces incubated in *S. epidermidis* in CDC biofilm reactor for 7 days. (1000 × , Scale bar = 20 μm).

adhesion (X–$OFP_{8.1}$ and X–$OFP_{13.6}$ vs. X–$OFP_{3.3}$). For *P. aeruginosa* adhesion, smooth materials reduction rates range from 57% to 81% while the textured surface material further reduce bacterial adhesion with reduction rates from 84% to 92% (Fig. 5C). Significantly lower adhesion was observed on textured X–$OFP_{13.6}$ comparing to textured X–$OFP_{3.3}$.

3.4. Biofilm formation assay on OFP and X–OFP surfaces

Biofilm formation assay was carried out in a CDC biofilm reactor and all materials were included in the same reactor to ensure all materials were exposed to same environment and conditions. Representative optical microscopy images of material surfaces after exposure to *S. epidermidis* culture for 7 days are shown in Fig. 6. Large biofilms were observed PU MS/0.4 smooth surfaces (Fig. 6A1-A2) and small patches of biofilm were occasionally observed on smooth OFP/X–OFP material surfaces, but much less than those observed on control PU MS/0.4 smooth surfaces. No biofilm formation was observed on textured material surfaces except for occasional bacterial aggregates. To examine biofilm structure, samples were observed under high magnification (Fig. 7). It is clear that biofilms formed on PU MS/0.4 surface consist of bacterial cells and extracellular polymeric substances (EPS) (Fig. 7A). Small biofilms were also observed on OFP smooth surface (Fig. 7B) while only bacterial cell clusters (Fig. 7C) or individual cells (Fig. 7D) were observed on X–$OFP_{13.6}$ smooth and textured surfaces respectively. Similar results of biofilm formation by *S. aureus* and *P. aeruginosa* were observed on PU MS/0.4 smooth surfaces while no biofilms were observed on textured X–OFP surfaces (Figs. 8–11). These results suggest that crosslinked X-OFPs significantly reduced bacterial adhesion and aggregation, and surface texturing further minimizes the bacteria aggregation, thereby inhibiting biofilm formation.

4. Discussion

Polyphosphazenes are high polymers with a linear backbone of alternating *P*–N atoms. The chemical structure of the backbone gives polyphosphazene a surprising high torsional freedom and a correspondingly high chain flexibility [20]. However, such inherently soft mechanical property also limits the application of polyphosphazenes in healthcare, generally like the soft materials studied in other fields [34,35]. Polymer mechanical properties can be improved via crosslinking. The introduction of allphenoxy groups into octafluoropentoxy side unit attached to the *P*–N backbone make the OFP polymer crosslinkable. By exposure of the polymer to UV radiation in the presence of a photosensitizer (AIBN in this study), the induced cycloaddition reaction of carbon-carbon double bonds on allphenoxy groups leads to the formation of crosslinking (Scheme 1). Alternatively, the formation of crosslinking could also be achieved by recombination of macroradicals. Upon exposure to UV radiation, the photosensitizer forms radicals and reacts with the double bonds on the polymer chains forming macroradicals. When two adjacent macroradicals annihilate by recombination, covalent bonds form between different polymer chains, forming the crosslinking. Our previous study shows that the crosslinking largely enhanced the mechanical strengths and the increase in stiffness further reduced bacterial adhesion [31]. This study focuses on the fabrication of textured X–OFP films using a variety of modified X-OFPs and bacterial responses to these new material surfaces.

Textured X–OFP surfaces can be fabricated with nanostructured patterns via a two-stage soft lithography replication molding process. The choice of solvent is important for the fabrication of textured X–OFP films. Using DMAC as solvent we have successfully fabricated submicron textured polyurethane (PU MS/0.4) biomaterial surfaces with a pillar yield of more than 99.8% [17]. However, in this study, when we used DMAC as solvent to fabricate the textured films we found many defects in pillars (Fig. 1A). This is probably due to the low evaporation rate of the solvent. DMAC has the highest boiling point compared to other solvents (DMF, THF and MEK) and evaporates slowly. When the additional layer of polymer was applied on the first thin film layer, the dried polymer layer may re-dissolve or be swelled by solvent to weaken the mechanical strength of pillars, resulting in pillar defects such as collapse. A similar phenomenon was also observed on DMF-polymer films although the structures formed better than with DMAC-polymer film (Fig. 1B). On the contrary, solvents in THF- and MEK- polymer solutions evaporate fast and the additional layers dry quickly. As a

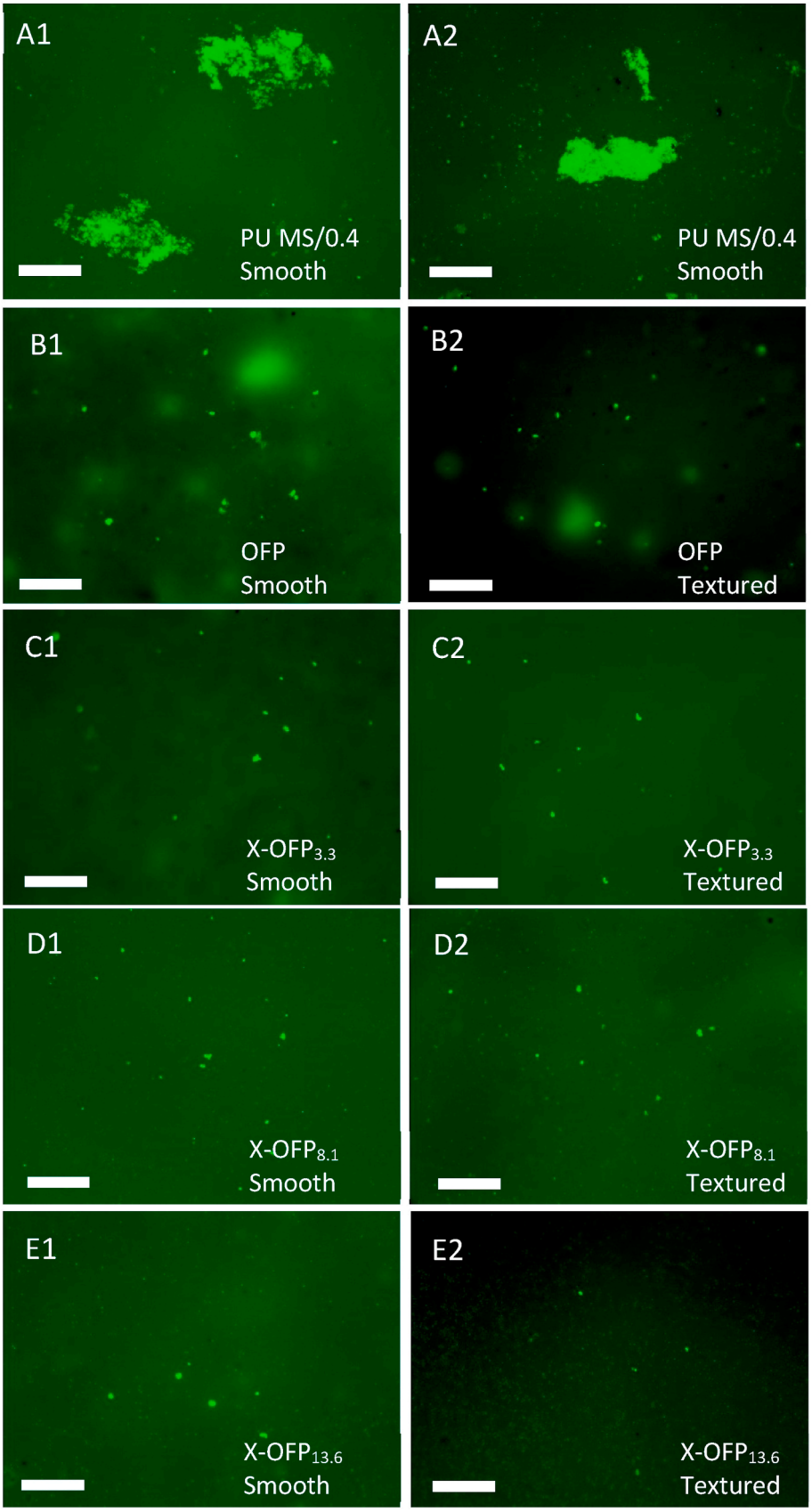

Fig. 8. Representative fluorescence images of material surfaces incubated in *S. aureus* culture in CDC biofilm reactor for 7 days. (A1, A2) PU MS/0.4 smooth, (B1, B2) OFP, (C1, C2) X–$OFP_{3.3}$, (D1, D2) X–$OFP_{8.1}$, (E1, E2) X–$OFP_{13.6}$. The textured surfaces were patterned with 500/500/600 nm pillars. (200 × , Scale bar = 50 μm).

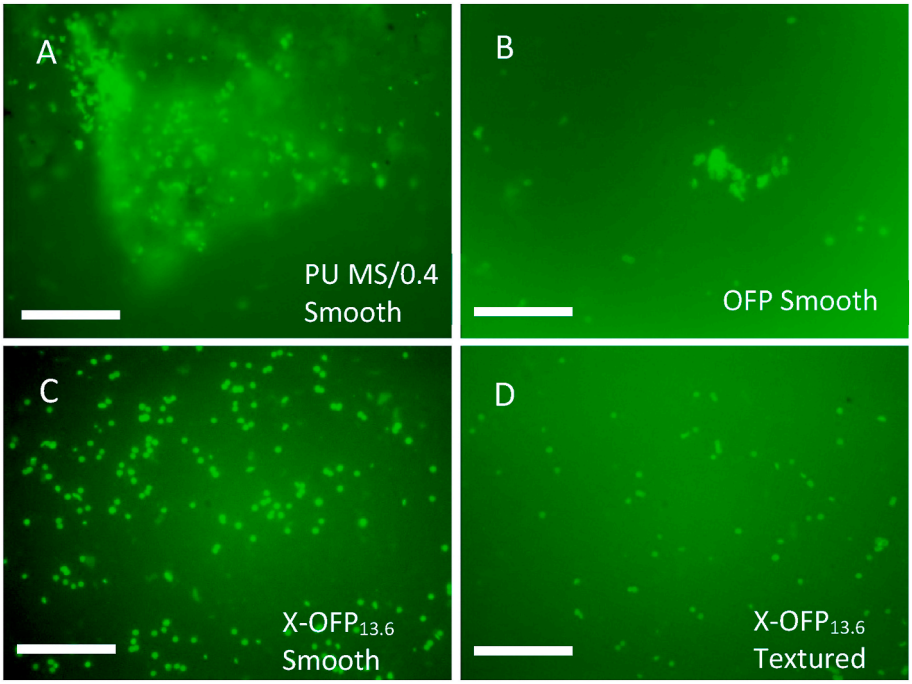

Fig. 9. Magnified fluorescence microscopy images of biofilms formed on (A) PU MS/0.4 smooth, (B) OFP smooth, (C) X–$OFP_{13.6}$ smooth and (D) X–$OFP_{13.6}$ textured surfaces incubated in *S. aureus* culture in CDC biofilm reactor for 7 days. (1000 ×, Scale bar = 20 μm).

result, intact films without pillar defects were obtained using THF or MEK solvents (Fig. 1C and D). However, the fast evaporation rate of solvent may also lead to non-uniform films. The THF-film appeared to have non-uniform thickness and structure due to the fast evaporation, while MEK-film appeared uniform and clear. The other reason for good quality of MEK-film may be due to the more uniform distribution of MEK throughout the polymers, as was confirmed in a triblock copolymer [36]. Taken together we conclude that MEK is the best solvent for fabrication of textured polyphosphazene films among the four commonly used solvents tested.

AFM was used to characterize the textured pillar patterns since no sample pretreatment is necessary. AFM provides surface topography images of sample directly through probe scanning, but also the pattern features can be quantified, including pillar diameter, pillar height, and pillar yield as well as the stiffness. The pillar yield and quality of textured polyphosphazene films are dependent on the mechanical properties of materials. A previous study showed that the elastic modulus of OFP measure by AFM nano-indentation technique was approximately 0.076 GPa and the introduction of crosslinking functional groups increased the modulus of materials after crosslinking, with the modulus of X–$OFP_{13.6}$ increasing to 0.171 GPa, about 2.25 times higher than OFP. Results also showed that the modulus increased with the density of crosslinking groups in X-OFPs [31]. In this study we found more pillar defects in textured OFP film surfaces than X-OFPs and the pillar yields increased with the crosslinking levels (Fig. 2). The pillar yield in X–$OFP_{13.6}$ surfaces reached 99.7% with 0.27% pillar defects, almost the same as the pillar yield (99.8%) of PU MS/0.4 films with the same textured pattern [17]. Since the mechanical strength increased with the increase of crosslinking density, we expect the mechanical properties of X–OFP can be further improved and the pillar yield can be raised over 99.8% if the crosslinking density is further increased. The related polymer is being developed and will be studied in the future. Pillar yield and quality of textured patterns are related to the pillar geometry including pillar diameter, pillar separation distance, and height. Large lateral size or shorter pillars are more likely to make the pillar more mechanically robust, leading to fewer defects of pillars, while small lateral size and high aspect ratio pillars are likely to produce more defects of pillars (e.g., collapse) due to weak mechanical properties. In addition, pillar dimensions change the surface contact area for bacterial interaction and surface hydrophobicity, causing different bacterial adhesion responses. Biomimetic studies show that surface structures are most effective in the range of 50–90% of the size of settling organisms [37] and that nanocylinder heights should be > 160 nm [38]. In this study, the pillar size 500/500/600 nm was selected to minimize the surface contact area and keep the distance between pillars to less than 1 μm, ensuring minimal bacterial cells will be captured between pillars. Results show that this pillar pattern is effective in controlling bacterial adhesion and biofilm formation (Figs. 5 and 6) although its efficiency might be improved through further optimization of the pattern. The effect of pillar pattern sizes on bacterial adhesion and optimization of patterns would be a topic for future studies.

Bacterial adhesion to material surfaces is the first critical step in biofilm-related biomaterial associated infection. Biomaterial surface properties such as surface chemistry, wettability, and topography are the main determinant factors influencing bacterial adhesion [39]. OFP and X–OFP are new polyphosphazene elastomers that show antibacterial properties without addition or incorporation of any antibiotics/biocides. The low bacterial adhesion on these polymeric surfaces is believed to be due to its fluorocarbon chemistry and low surface energy. It has been reported that the linear backbone polymers containing fluorocarbon side chains can be non-sticking coatings for inhibition of bacterial adhesion [40]. An early *in vitro* adhesion study of twenty nine *S. epidermidis* strains to Teflon, polyethylene and polycarbonate showed low adhesion to polymers with a low surface free energy [41]. OFP and X–OFP materials resemble classical fluorocarbon polymers such as Teflon and have a water contact angle around 93–97° and low surface energy, leading to low bacterial adhesion. A similar result can also be seen with another elastomer with a similar structure, polyphosphazene fluoroelastomer (PNF). PNF has been approved as dental liner material because of its antimicrobial characteristics and its unusual impact-absorbing qualities [42,43]. All of these suggest that side groups with fluorocarbon chemistry in polyphosphazenes can be a chemical structure with antibacterial potential and without causing antibiotic resistance. Furthermore, unlike Teflon, OFP and X-OFPs are

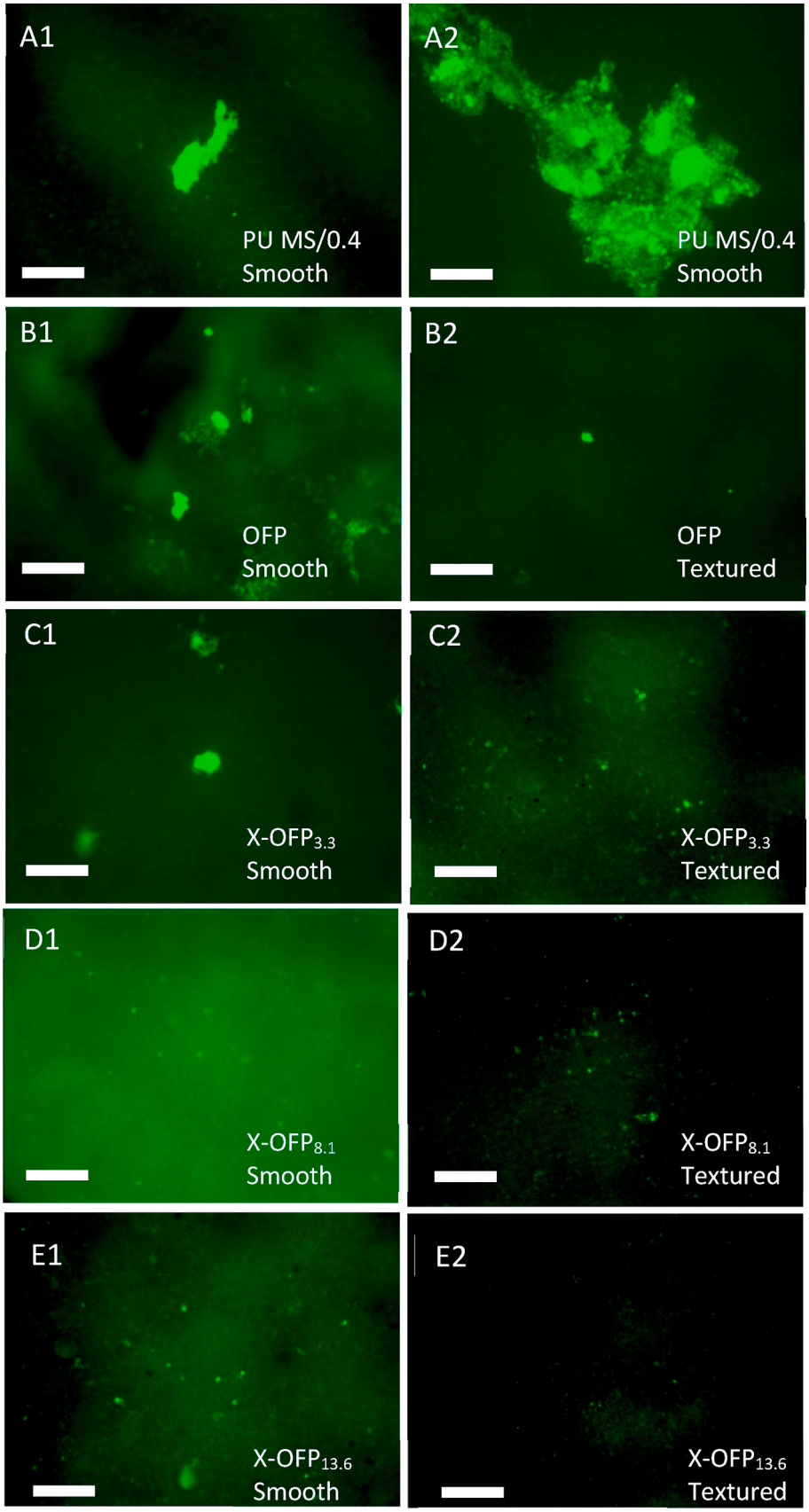

Fig. 10. Representative fluorescence images of material surfaces incubated in *P. aeruginosa* culture in CDC biofilm reactor for 7 days. (A1, A2) PU MS/0.4 smooth, (B1, B2) OFP, (C1, C2) X–$OFP_{3.3}$, (D1, D2) X–$OFP_{8.1}$, (E1, E2) X–$OFP_{13.6}$. The textured surfaces were patterned with 500/500/600 nm pillars. (200 × , Scale bar = 50 μm).

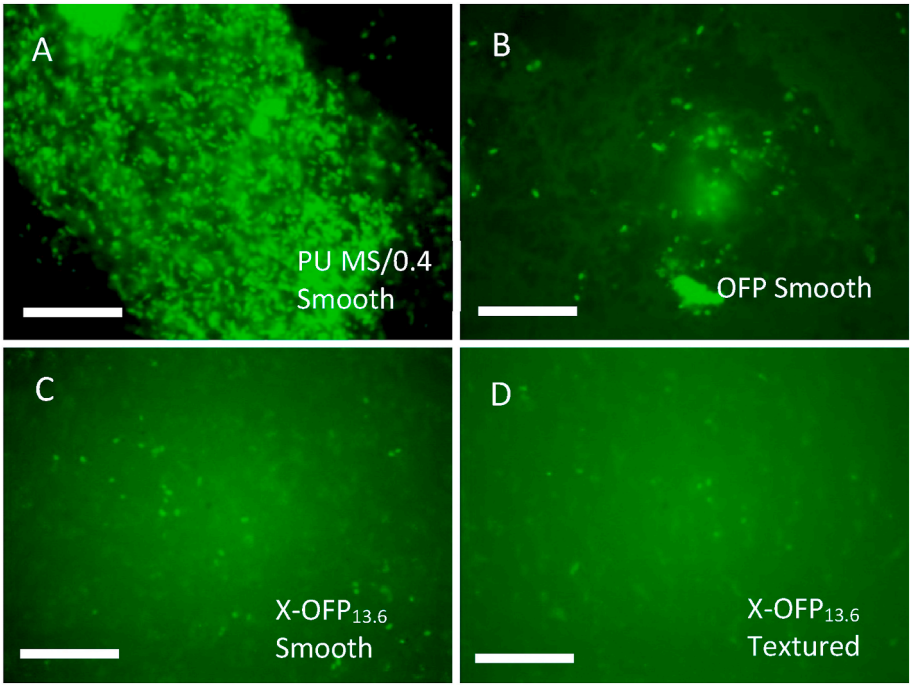

Fig. 11. Magnified fluorescence microscopy images of biofilms formed on (A) PU MS/0.4 smooth, (B) OFP smooth, (C) X–OFP$_{13.6}$ smooth and (D) X–OFP$_{13.6}$ textured surfaces incubated in *P. aeruginosa* culture in CDC biofilm reactor for 7 days. (1000 × , Scale bar = 20 μm).

soluble in some organic solvents and they can be solution-cast into films, making them ideal for fabrication of medical devices and further surface topographical modification.

Physical surface topography modification with texturing of the submicron pillars enhances the antibacterial properties. Submicron texturing reduces the surface accessible contact area for the interaction with bacterial cells. The fractions of total top surface areas for 500/500/600 nm textured patterns are ~25% of the nominal surface area [17]. The surface texturing also makes the hydrophobic substrate surface more hydrophobic by air entrapped in-between surface structures though the Cassie-Baxter effect. The creation of an air-liquid interfaces blocks bacteria from accessing the material surface thereby limiting the bacterial attachment [44]. Our previous studies have demonstrated that textured polyurethane surfaces inhibited staphylococcal bacterial adhesion and biofilm formation [17,18]. In this study the textured X–OFP surfaces exhibited significantly lower bacterial adhesion than on the corresponding smooth surfaces for three strains, suggesting that Cassie-Baxter wetting state is effective for the adhesion of both Gram-negative and Gram-positive bacteria (Fig. 5). The individual bacterial adhesion onto textured X–OFP surfaces is also dependent on the crosslinking level of X-OFPs. High crosslinking level causes low adhesion. This is probably due to the rigidity of pillars and the decrease in defects that come with increased crosslinking. A previous study showed lower bacterial adhesion on rigid crosslinked X–OFP surface than on the less rigid materials pre-crosslinking, indicating mechanical stiffness may be an important parameter influencing bacterial attachment [31]. The high crosslinking level also decreased the defects of pillars in textured patterns, where bacterial cells are easier to attach and colonize on surfaces. X–OFP$_{13.6}$ produced textured surfaces with ~0.27% defects, less than on X–OFP$_{3.3}$ and X–OFP$_{8.1}$ surfaces. Thus, significantly lower bacterial adhesion was observed on the textured surface with high crosslinking density (e.g., X–OFP$_{13.6}$, Fig. 5). It should be noted that no statistically significant differences in adhesion between textured X–OFP$_{3.3}$ and OFP surfaces were observed, most likely due to the small increase in stiffness and the similar chemistry between X–OFP$_{3.3}$ and OFP. The other potential reason is due to the increase in defects on both textured X–OFP$_{3.3}$ and OFP surfaces compared to X–OFP$_{8.1}$ and X–OFP$_{13.6}$.

The resistance to microbial infection by textured X–OFP surfaces is also seen in the resistance to biofilm formation. No biofilms were observed on textured X–OFP surfaces after incubation in a CDC biofilm reactor for 7 days for all three strains, especially for the X–OFP$_{13.6}$ with high crosslinking level. Significant biofilm or small patch of biofilms were observed on PU MS/0.4 or OFP smooth surfaces (Figs. 6A, 7A and 7B and supplement Figures 1-4). The “slime” or extracellular polymeric substances (EPS) can be observed forming the biofilm matrix on PU MS/0.4 or OFP smooth surfaces, while only individual bacterial cells or small clusters were observed on textured X–OFP surfaces, suggesting the textured patterns inhibit the production of EPS. As the main component of biofilms, EPS play a vital role in biofilm formation and also function as barriers to protect the cells against the attacks from environment such as antibiotics [45]. Results suggest that the textured X–OFP surfaces inhibit biofilm formation on biomaterials and reduce EPS production, which may increase the efficacy of antibiotics in controlling microbial infection. Although the experiment duration for biofilm formation was only assessed at 7 days in this study, our previous study has shown no biofilms formed on a textured X–OFP surface for 23 days under shear [30]. We can expect that textured X-OFPs with high crosslinking level (e.g., X–OFP$_{13.6}$) will inhibit microbial biofilm formation for longer times, which will be studied in future.

5. Conclusions

Textured fluorinated alkoxyphosphazene (X–OFP) films with submicron ordered pillars were successfully fabricated using MEK as solvent and via a two stage soft lithography replication molding process. The quality of the textured pattern is related to the solvent and mechanical properties of the materials. High crosslinking density increased the mechanical stiffness of X-OFPs and decreased the defects in pillars. OFP and X-OFPs are resistant to bacterial adhesion of *S. epidermidis*, *S. aureus* and *P. aeruginosa*, and surface texturing further enhances the antibacterial properties. Moreover, the resistance to bacterial adhesion shows a positive relationship with the crosslinking degrees. Combining the surface fluorocarbon chemistry, low surface energy, and submicron

textured surface topography, X-OFPs, especially X–$OFP_{13.6}$, exhibited excellent inhibition of biofilm formation, thereby improving the biocompatibility of current biomaterials with significant reduction in risk of pathogenic infection.

CRediT authorship contribution statement

Meixian Tang: Investigation, Visualization, Writing - original draft. **Chen Chen:** Methodology, Investigation. **Jieru Zhu:** Investigation. **Harry R. Allcock:** Conceptualization, Writing - review & editing. **Christopher A. Siedlecki:** Conceptualization, Supervision, Writing - review & editing. **Li-Chong Xu:** Methodology, Investigation, Visualization, Writing - original draft, Formal analysis, Funding acquisition.

Declaration of competing interest

The authors declare that they have no known competing financial interests or personal relationships that could have appeared to influence the work reported in this paper.

Acknowledgements

Research reported in this publication was supported by the National Institute of Allergy and Infectious Disease of NIH under award number R21 AI139706.

References

[1] C.R. Arciola, D. Campoccia, L. Montanaro, Implant infections: adhesion, biofilm formation and immune evasion, Nat. Rev. Microbiol. 16 (2018) 397–409.
[2] S.S. Magill, J.R. Edwards, W. Bamberg, Z.G. Beldavs, G. Dumyati, M.A. Kainer, et al., Multistate point-prevalence survey of health care–associated infections, N. Engl. J. Med. 370 (2014) 1198–1208.
[3] S.L. Percival, L. Suleman, C. Vuotto, G. Donelli, Healthcare-associated infections, medical devices and biofilms: risk, tolerance and control, J. Med. Microbiol. 64 (2015) 323–334.
[4] C.L. Ventola, The antibiotic resistance crisis: part 1: causes and threats, Pharmacy and Therapeutics 40 (2015) 277.
[5] G.M. Rossolini, F. Arena, P. Pecile, S. Pollini, Update on the antibiotic resistance crisis, Curr. Opin. Pharmacol. 18 (2014) 56–60.
[6] E. Martens, A.L. Demain, The antibiotic resistance crisis, with a focus on the United States, J. Antibiot. 70 (2017) 520–526.
[7] D. Campoccia, L. Montanaro, C.R. Arciola, A review of the biomaterials technologies for infection-resistant surfaces, Biomaterials 34 (2013) 8533–8554.
[8] J. Hasan, R.J. Crawford, E.P. Ivanova, Antibacterial surfaces: the quest for a new generation of biomaterials, Trends Biotechnol. 13 (2013) 295–304.
[9] E. Taylor, T.J. Webster, Reducing infections through nanotechnology and nanoparticles, Int. J. Nanomed. 6 (2011) 1463–1473.
[10] B. Ozcelik, K.K.K. Ho, V. Glattauer, M. Willcox, N. Kumar, H. Thissen, Poly(ethylene glycol)-based coatings combining low-biofouling and quorum-sensing inhibiting properties to reduce bacterial colonization, ACS Biomater. Sci. Eng. 3 (2017) 78–87.
[11] I. Francolini, I. Silvestro, V. Di Lisio, A. Martinelli, A. Piozzi, Synthesis, characterization, and bacterial fouling-resistance properties of polyethylene glycol-grafted polyurethane elastomers, Int. J. Mol. Sci. 20 (2019) 1001.
[12] M. Colilla, I. Izquierdo-Barba, M. Vallet-Regí, The role of zwitterionic materials in the fight against proteins and bacteria, Medicines (Basel) 5 (2018) 125.
[13] K.A. Whitehead, J. Colligon, J. Verran, Retention of microbial cells in substratum surface features of micrometer and sub-micrometer dimensions, Colloids Surf. B Biointerfaces 41 (2005) 129–138.
[14] K. Anselme, P. Davidson, A.M. Popa, M. Giazzon, M. Liley, L. Ploux, The interaction of cells and bacteria with surfaces structured at the nanometre scale, Acta Biomater. 6 (2010) 3824–3846.
[15] E.P. Ivanova, J. Hasan, H.K. Webb, V.K. Truong, G.S. Watson, J.A. Watson, et al., Natural bactericidal surfaces: mechanical rupture of Pseudomonas aeruginosa cells by cicada wings, Small 8 (2012) 2489–2494.
[16] E.P. Ivanova, J. Hasan, H.K. Webb, G. Gervinskas, S. Juodkazis, V.K. Truong, et al., Bactericidal activity of black silicon, Nat. Commun. 4 (2013) 2838.
[17] L.-C. Xu, C.A. Siedlecki, Submicron-textured biomaterial surface reduces staphylococcal bacterial adhesion and biofilm formation, Acta Biomater. 8 (2012) 72–81.
[18] L.-C. Xu, C.A. Siedlecki, Staphylococcus epidermidis adhesion on hydrophobic and hydrophilic textured biomaterial surfaces, Biomed. Mater. 9 (2014) 035003.
[19] K.R. Milner, A.J. Snyder, C.A. Siedlecki, Sub-micron texturing for reducing platelet adhesion to polyurethane biomaterials, J. Biomed. Mater. Res. 76A (2006) 561–570.
[20] H.R. Allcock, The expanding field of polyphosphazene high polymers, Dalton Trans. 45 (2016) 1856–1862.
[21] H.R. Allcock, N.L. Morozowich, Bioerodible polyphosphazenes and their medical potential, Polym. Chem. 3 (2012) 578–590.
[22] Z. Tian, Y. Zhang, X. Liu, C. Chen, M.J. Guiltinan, H.R. Allcock, Biodegradable polyphosphazenes containing antibiotics: synthesis, characterization, and hydrolytic release behavior, Polym. Chem. 4 (2013) 1826–1835.
[23] A. Lutzke, B.H. Neufeld, M.J. Neufeld, M.M. Reynolds, Nitric oxide release from a biodegradable cysteine-based polyphosphazene, J. Mater. Chem. B 4 (2016) 1987–1998.
[24] A. Lutzke, J.B. Tapia, M.J. Neufeld, M.M. Reynolds, Sustained nitric oxide release from a tertiary S-Nitrosothiol-based polyphosphazene coating, ACS Appl. Mater. Interfaces 9 (2017) 2104–2113.
[25] D. Capodanno, C. Tamburino, Properties and clinical development of a novel coating technology: the poly [bis (trifluoroethoxy) phosphazene], Recent Pat. Drug Deliv. Formulation 4 (2010) 18–22.
[26] A. Welle, M. Grunze, D. Tur, Plasma protein adsorption and platelet adhesion on poly[bis(trifluoroethoxy)phosphazene] and reference material surfaces, J. Colloid Interface Sci. 197 (1998) 263–274.
[27] C. Henn, S. Satzl, P. Christoph, P. Kurz, B. Radeleff, U. Stampfl, et al., Efficacy of a polyphosphazene nanocoat in reducing thrombogenicity, in-stent stenosis, and inflammatory response in porcine renal and iliac artery stents, J. Vasc. Intervent. Radiol. 19 (2008) 427–437.
[28] S. Satzl, C. Henn, P. Christoph, P. Kurz, U. Stampfl, S. Stampfl, et al., The efficacy of nanoscale poly [bis (trifluoroethoxy) phosphazene](PTFEP) coatings in reducing thrombogenicity and late in-stent stenosis in a porcine coronary artery model, Invest. Radiol. 42 (2007) 303–311.
[29] Y. Huang, X. Liu, L. Wang, S. Li, E. Verbeken, I. De Scheerder, Long-term biocompatibility evaluation of a novel polymer-coated stent in a porcine coronary stent model, Coron. Artery Dis. 14 (2003) 401–408.
[30] L.-C. Xu, Z. Li, Z. Tian, C. Chen, H.R. Allcock, C.A. Siedlecki, A new textured polyphosphazene biomaterial with improved blood coagulation and microbial infection responses, Acta Biomater. 67 (2018) 87–98.
[31] L.-C. Xu, C. Chen, J. Zhu, M. Tang, A. Chen, H.R. Allcock, et al., New cross-linkable poly[bis(octafluoropentoxy) phosphazene] biomaterials: synthesis, surface characterization, bacterial adhesion, and plasma coagulation responses, J. Biomed. Mater. Res. B Appl. Biomater. (2020) n/a:in press.
[32] W.L. Hergenrother, A.F. Halasa, Polyphosphazene Polymers Containing Alkoxy Substituents Containing a Fully Substituted Carbon in the Beta Position, (1981) USA.
[33] J. Drelich, E. Chibowski, Superhydrophilic and superwetting surfaces: definition and mechanisms of control, Langmuir 26 (2010) 18621–18623.
[34] H.R. Allcock, Polyphosphazene elastomers, gels, and other soft materials, Soft Matter 8 (2012) 7521–7532.
[35] H.R. Allcock, Polyphosphazenes as an example of the element-blocks approach to new materials, in: Y. Chujo (Ed.), New Polymeric Materials Based on Element-Blocks, Springer Singapore, Singapore, 2019, pp. 167–188.
[36] S. Xiong, D. Li, S.-M. Hur, G.S.W. Craig, C.G. Arges, X.-P. Qu, et al., The solvent distribution effect on the self-assembly of symmetric triblock copolymers during solvent vapor annealing, Macromolecules 51 (2018) 7145–7151.
[37] A.J. Scardino, R. de Nys, Mini review: biomimetic models and bioinspired surfaces for fouling control, Biofouling 27 (2011) 73–86.
[38] D. Campoccia, L. Montanaro, H. Agheli, D.S. Sutherland, V. Pirini, M.E. Donati, et al., Study of Staphylococcus aureus adhesion on a novel nanostructured surface by chemiluminometry, Int. J. Artif. Organs 29 (2006) 622–629.
[39] L.-C. Xu, C.A. Siedlecki, Bacterial adhesion and interaction with biomaterial surfaces, in: D.W. Hutmacher, W. Chrzanowski (Eds.), Biointerfaces: where Material Meets Biology, The Royal Society of Chemistry, Cambridge, UK, 2015, pp. 365–398.
[40] J. Tsibouklis, M. Stone, A. Thorpe A, P. Graham, T.G. Nevell, R.J. Ewen, Inhibiting bacterial adhesion onto surfaces: the non-stick coating approach, Int. J. Adhesion Adhes. 20 (2000) 91–96.
[41] C.M. Ferreirós, J. Carballo, M.T. Criado, V. Sáinz, M.C. del Río, Surface free energy and interaction of Staphylococcus epidermidis with biomaterials, FEMS (Fed. Eur. Microbiol. Soc.) Microbiol. Lett. 60 (1989) 89–94.
[42] L. Gettleman, L. Ross-Bertrand, P.H. Gebert, L.R. Guerra, Novel Elsstomers for Denture and Maxillofacial Prostheses Biomedical Engineering IV, Pergamon, 1985, pp. 141–144.
[43] L. Gettleman, J.M. Vargo, P.H. Gebert, C.L. Farris, R.J. LeBoeuf, H.R. Rawls, Polyphosphazine fluoroelastomer (PNF) as a permanent soft liner for removable dentures, in: C.G. Gebelein (Ed.), Advances in Biomedical Polymers, Springer US, Boston, MA, 1987, pp. 55–61.
[44] Y. Cheng, G. Feng, C.I. Moraru, Micro- and nanotopography sensitive bacterial attachment mechanisms: a review, Front. Microbiol. 10 (2019).
[45] J. Wingender, T.R. Neu, H.-C. Flemming, What are bacterial extracellular polymeric substances? in: J. Wingender, T.R. Neu, H.-C. Flemming (Eds.), Microbial Extracellular Polymeric Substances: Characterization, Structure and Function, Springer Berlin Heidelberg, Berlin, Heidelberg, 1999, pp. 1–19.